

1 **Epigenetic targeting of PGBD5-dependent DNA damage in SMARCB1-deficient sarcomas**

2

3 Yaniv Kazansky^{1,2}, Helen S. Mueller^{1,2}, Daniel Cameron^{1,2}, Phillip Demarest^{1,2}, Nadia Zaffaroni³,
4 Noemi Arrighetti³, Valentina Zuco³, Prabhjot S. Mundi⁴, Yasumichi Kuwahara⁵, Romel Somwar⁶,
5 Rui Qu⁷, Andrea Califano⁸, Elisa de Stanchina⁷, Filemon S. Dela Cruz⁸, Andrew L. Kung⁸, Mrinal
6 M. Gounder⁹, Alex Kentsis^{1,2,10*}

7

8 ¹ Molecular Pharmacology Program, Sloan Kettering Institute, Memorial Sloan Kettering Cancer
9 Center, New York, NY, USA

10 ² Tow Center for Developmental Oncology, Department of Pediatrics, Memorial Sloan Kettering
11 Cancer Center, New York, NY, USA

12 ³ Molecular Pharmacology Unit, Department of Experimental Oncology, Fondazione IRCCS
13 Istituto Nazionale dei Tumori di Milano, Milan, Italy

14 ⁴ Department of Systems Biology, Columbia University Irving Medical Center, New York, NY, USA

15 ⁵ Department of Biochemistry and Molecular Biology, Kyoto Prefectural University of Medicine

16 ⁶ Department of Pathology, Memorial Sloan Kettering Cancer Center, New York, NY, USA

17 ⁷ Antitumor Assessment Core, Memorial Sloan Kettering Cancer Center, New York, NY, USA

18 ⁸ Department of Pediatrics, Memorial Sloan Kettering Cancer Center, New York, NY, USA

19 ⁹ Department of Medicine, Memorial Sloan Kettering Cancer Center, New York, NY, USA

20 ¹⁰ Departments of Pediatrics, Pharmacology, and Physiology & Biophysics, Weill Medical College
21 of Cornell University, New York, NY, USA

22

23 * Correspondence: Alex Kentsis, MD, PhD, email kentsisresearchgroup@gmail.com, telephone
24 +1-646-888-2593, 1275 York Avenue, ZRC-1863, New York, NY 10021

25

26 Running title: Epigenetic targeting of DNA damage

27 Keywords: epigenetics, EZH2 inhibition, BAF, combination therapy, PRC2

28

29

30 **Conflict of Interest**

31 The authors declare no potential conflicts of interest. AK is a consultant for Novartis, Rgenta,
32 Blueprint, and Syndax.

33

34

35

36 **Abstract**

37 Despite the potential of targeted epigenetic therapies, most cancers do not respond to current
38 epigenetic drugs. The Polycomb repressive complex EZH2 inhibitor tazemetostat was recently
39 approved for the treatment of *SMARCB1*-deficient epithelioid sarcomas, based on the functional
40 antagonism between PRC2 and loss of *SMARCB1*. Through the analysis of tazemetostat-
41 treated patient tumors, we recently defined key principles of their response and resistance to
42 EZH2 epigenetic therapy. Here, using transcriptomic inference from *SMARCB1*-deficient tumor
43 cells, we nominate the DNA damage repair kinase ATR as a target for rational combination
44 EZH2 epigenetic therapy. We show that EZH2 inhibition promotes DNA damage in epithelioid
45 and rhabdoid tumor cells, at least in part via its induction of the transposase-derived PGBD5.
46 We leverage this collateral synthetic lethal dependency to target PGBD5-dependent DNA
47 damage by inhibition of ATR but not CHK1 using elimusertib. Consequently, combined EZH2
48 and ATR inhibition improves therapeutic responses in diverse patient-derived epithelioid and
49 rhabdoid tumors *in vivo*. This advances a combination epigenetic therapy based on EZH2-
50 PGBD5 synthetic lethal dependency suitable for immediate translation to clinical trials for
51 patients.

52

53

54 Introduction

55

56 Targeted epigenetic therapies offer potential improvements over conventional cytotoxic
57 chemotherapies through superior clinical efficacy and reduced toxicity. In cancers caused by
58 genetic mutations of transcriptional and epigenetic regulators, specific inhibition of epigenetic
59 effectors can directly block dysregulated gene expression by leveraging cancer-specific
60 dependencies. One promising example of this therapeutic approach is in cancers caused by
61 mutation of the chromatin remodeling SWI/SNF/BAF (Brg/Brahma-associated factors) complex,
62 a ubiquitous epigenetic regulator that is mutated in at least 20% of human cancers (1). In
63 particular, the highly lethal solid tumors caused by loss of the core BAF subunit *SMARCB1* (2-4),
64 which include malignant rhabdoid tumors (MRT) and epithelioid sarcomas (ES), are known to be
65 dependent on the methyltransferase EZH2, a component of the Polycomb Repressive Complex
66 2 (PRC2). This dependency is thought to result from epigenetic antagonism between BAF and
67 PRC2, in which normal BAF activity evicts PRC2 from tumor suppressor loci (5, 6). In a recent
68 clinical trial, this dependency was targeted using the EZH2 methyltransferase inhibitor
69 tazemetostat (TAZ), leading to its FDA approval (7). Yet despite the promise of this therapeutic
70 approach, EZH2 inhibition as a monotherapy exhibited efficacy in only a subset of patients, with
71 most patient tumors having either primary resistance or acquiring resistance after treatment (7,
72 8). Thus, there is a critical need to develop improved epigenetic combination therapies, which can
73 be achieved at least in part through improved understanding of the effects of EZH2 inhibition in
74 epithelioid and rhabdoid tumors.

75

76 We recently leveraged functional genomics of epithelioid and rhabdoid tumors to elucidate the
77 mechanisms of resistance to EZH2 inhibition, including frequent disruption of the RB1/E2F cell
78 cycle control axis causing TAZ resistance in patients. This discovery led to the identification of
79 the AURKB inhibitor barasertib combination therapy that can overcome *RB1*-mediated TAZ
80 resistance *in vitro* and improve TAZ responses in preclinical epithelioid and rhabdoid tumor
81 xenografts *in vivo* (8). This approach bypasses primary and acquired RB1/E2F-mediated
82 checkpoint defects to maintain TAZ-induced reprogramming of oncogenic gene expression.
83 However, RB1/E2F pathway alterations were observed in less than half of epithelioid and
84 rhabdoid tumors, raising the question of additional combinations that may achieve effective
85 epigenetic therapy for patients, including those with primary or acquired TAZ resistance.

86

87 Epithelioid and rhabdoid tumors occur due to characteristic biallelic deletions and inactivating
88 mutations of *SMARCB1*, either as a result of germline rhabdoid tumor predisposition syndrome,
89 or due to somatic mutations (2, 9, 10). For rhabdoid tumors, differences in the types of mutations,
90 e.g. large versus small chromosomal deletions or missense and nonsense mutations of
91 *SMARCB1* correspond with distinct molecular subtypes and clinical features (11). Genome
92 sequencing studies have identified distinct sequence-specific mutational features in rhabdoid
93 tumors, including sequence-specific deletions of *SMARCB1* and recurrent mutations of other
94 genes, associated at least in part with the mutagenic activity of the domesticated transposase-
95 derived Piggybac Transposable Element Derived 5 (PGBD5) (9).

96
97 PGBD5 is among the most evolutionarily conserved domesticated transposase-derived genes in
98 vertebrates and can mediate sequence-specific DNA rearrangements dependent on its putative
99 nuclease activity (9, 12). In particular, Pgbd5 promotes sequence-specific somatic mutagenesis
100 and tumor development in mouse models of medulloblastoma, one of the most common childhood
101 brain tumors (13). PGBD5-expressing cells, including rhabdoid tumor cells, require a distinct form
102 of non-homologous end-joining (NHEJ) DNA repair, leading to their hypersensitivity to inhibition
103 of DNA repair signaling, specifically ATR inhibition (14). We have now found that TAZ inhibition
104 of EZH2 can increase PGBD5 expression in epithelioid and rhabdoid tumor cells, potentiating
105 PGBD5-dependent DNA damage, and conferring synergy with the ATR-selective DNA repair
106 inhibitor elimusertib. Accordingly, combined treatment of patient-derived rhabdoid and epithelioid
107 tumors engrafted into immunodeficient mice, including from patients with multiply relapsed
108 metastatic disease, demonstrates synergistic activity *in vivo*.

109

110 **Results**

111

112 To define potential therapeutic targets for TAZ combination therapy in *SMARCB1*-deficient
113 tumors, we leveraged a recently developed method for transcriptomic inference of oncogenic
114 protein activity, termed metaVIPER (Virtual Inference of Protein activity by Enriched Regulon), as
115 applied to gene expression profiles of 68 patient rhabdoid tumors (15-17). We used the
116 OncoTarget annotation of high-affinity pharmacologic inhibitors of putative master gene
117 expression regulators (MRs) to order them by their mean activity scores (**Figure 1A**). As
118 expected, EZH2 was among the most activated MR proteins in rhabdoid tumors, as was the
119 previously identified TAZ combination therapy target, AURKB (**Figure 1A**). This analysis also
120 prioritized CDK4, CDK2, and AURKA (**Figure 1A**), consistent with the previously established

121 activity of cell cycle checkpoints downstream of G1/S in rhabdoid tumors (8), validating this
122 ranking approach.

123

124 In addition to these known dependencies, this analysis also identified the NHEJ DNA repair
125 structural factor XRCC6 (Ku70), and its mediator kinase ATR among the most activated MR
126 genes among all 6,000 MR proteins in metaVIPER (**Figure 1B**), both of which have been shown
127 to be required for the survival of cells expressing active PGBD5 in prior studies (14). Indeed,
128 XRCC6 ranked higher in this analysis than the well-validated target EZH2 (**Figure 1B**).

129

130 To ascertain the robustness of this prediction, we next analyzed an independent dataset from
131 Kuster and colleagues (18), which assessed the responses of sarcoma cell lines to a panel of 151
132 pharmacologic inhibitors, including G401 and A204 rhabdoid tumor and VA-ES-BJ epithelioid
133 sarcoma cell lines. We observed that the ATR-selective kinase inhibitor elimusertib was among
134 the most active drugs against epithelioid and rhabdoid tumor cells, even more active than both
135 TAZ and barasertib (**Figure 1C**). Thus, *SMARCB1*-deficient epithelioid and rhabdoid tumors are
136 highly sensitive to ATR inhibition (14).

137

138 Since both modulation of gene expression by TAZ and DNA repair by ATR inhibitor elimusertib
139 appears to have prominent activity in rhabdoid tumor cells, we inquired whether TAZ may regulate
140 PGBD5 itself. We found that in addition to the expected upregulation of Polycomb gene sets,
141 EZH2 inhibition in G401 rhabdoid tumor cells with TAZ for 11 days also caused a significant
142 increase in the expression of *PGBD5* (mean fold-increase of 6.6 and Student's t-test $p = 1.2E-7$;
143 **Figure 1D**). Using CRISPR gene editing, we generated isogenic *RB1* wild-type and *RB1^{del}* mutant
144 G401 cells and confirmed correct biallelic *RB1* inactivating mutations and consequent loss of RB1
145 protein expression, using the *AAVS1* safe harbor as a negative control (8). In prior work, we found
146 that defects in the RB1/E2F axis, including mutations of *RB1*, cause TAZ resistance (8).
147 Consistent with the independence of this TAZ resistance mechanism from ATR inhibitor
148 susceptibility, two independent G401 *RB1^{del}* mutant cell lines also exhibited significant TAZ-
149 mediated induction of *PGBD5* expression (mean fold-increase of 333 and 8.6 and t-test $p = 1.3E-$
150 6 and $1.6E-6$ for E1 and F2 clones, respectively; **Figure 1D**). Additionally, both *RB1^{WT}* and *RB1^{del}*
151 mutant G401 cells exhibited nanomolar susceptibility to the ATR-selective inhibitor elimusertib
152 (half-maximal effective concentration of 18 ± 1.6 nM, 19 ± 3.8 nM, and 27 ± 3.2 nM for *RB1^{WT}*,
153 *RB1^{del}* E1, and F2 clones, respectively; **Figure 1E**).

154

155 Elimusertib is currently undergoing clinical trials in patients with refractory or relapsed solid
156 tumors, including patients with *PGBD5*-expressing tumors such as MRT and ES (Clinical Trials
157 Identifier NCT05071209). We therefore investigated the activity of combination treatment with
158 TAZ and elimusertib, reasoning that TAZ-induced upregulation of *PGBD5* expression may
159 potentiate the anti-tumor effects of ATR inhibition. We observed greater antitumor effects from
160 the combination of TAZ and elimusertib than either drug alone against diverse MRT and ES cell
161 lines, including TAZ-resistant ES1 and VAESBJ cells (mean fold-decrease in normalized cell
162 viability of 0.64, 0.63, 0.78, 0.84, and 0.84 compared with most effective monotherapy for
163 TTC642, KP-MRT-NS, KP-MRT-RY, G401 and ES1 respectively, *t*-test 1.0E-3, 3.0E-5, 3.3E-3,
164 2.6E-4, and 6.1E-5 ;**Figure 2A**). Strikingly, the combination of TAZ and elimusertib was highly
165 synergistic in G401 rhabdoid and ES1 epithelioid sarcomas cells (ZIP synergy = 3.4 and 2.0 and
166 $p = 9.8E-1$ and $7.3E-1$, respectively; **Figure 2B-C**).

167
168 If the improved anti-tumor activity of TAZ and elimusertib is due to the induction of *PGBD5*-
169 dependent DNA damage, then this treatment combination should be associated with the induction
170 of DNA damage repair signaling. To test this prediction, we used confocal immunofluorescence
171 microscopy to quantify γ H2AX as a specific marker of DNA damage (19). In agreement with prior
172 studies (14), vehicle-treated G401 cells showed measurable γ H2AX staining associated with
173 baseline *PGBD5* expression (**Figure 2D-E**). Consistent with TAZ-mediated induction of *PGBD5*
174 expression (**Figure 1D**), we found that TAZ treatment alone significantly increased nuclear γ H2AX
175 (mean normalized intensity = 0.42 versus 0.29 for TAZ and DMSO, respectively; *t*-test $p = 9.3E-$
176 3 ; **Figures 2D-E**). The combination of TAZ and elimusertib induced a significant increase in
177 γ H2AX as compared to either drug alone (mean normalized intensity = 1.8 for the combination
178 versus 0.42 and 0.85 for TAZ and elimusertib, respectively; *t*-test $p = 6.2E-14$ and $1.5E-29$ for
179 combination versus elimusertib and TAZ, respectively; **Figures 2D-E**).

180
181
182 Recently, EZH2 suppression was shown to induce replication stress through upregulation of
183 MYCN expression in T-ALL cells, which in turn sensitized cells to inhibition of CHK1 (19), a
184 downstream mediator of ATR signaling (20). To test this possibility, we measured *MYCN*
185 expression in TAZ-treated G401 rhabdoid tumor cells, which was significantly increased (**Figure**
186 **3A**). However, this induction of *MYCN* gene expression was not associated with the accumulation
187 of MYCN protein, as measured by Western blotting with *MYCN*-amplified IMR5 neuroblastoma
188 cells as a positive control (**Figure 3B**). Consistent with this, EZH2 inhibition either alone or in

189 combination with CHK1 inhibition did not induce apparent replication stress, as measured by RPA
190 phosphorylation, using the treatment of cells with the DNA topoisomerase inhibitor camptothecin
191 as positive control for replication stress. This was despite the effective inhibition of CHK1 auto-
192 phosphorylation by the CHK1-selective SRA737 inhibitor (**Figure 3C**). Concordantly, the CHK1
193 inhibitor SRA737 showed poor activity against G401 cells, regardless of *RB1* status (**Figure 3D**).
194 Thus, rhabdoid tumor cells exhibit a specific dependency on ATR-dependent but CHK1-
195 independent DNA damage repair signaling.

196

197 TAZ-mediated induction of *PGBD5* and DNA damage would indicate that this form of DNA
198 damage should be dependent on *PGBD5* expression. To test this prediction, we engineered short
199 hairpin RNA-mediated depletion of *PGBD5* in G401 cells using lentiviral transduction of two
200 independent *PGBD5*-specific shRNAs (sh*PGBD5*), as compared to a control GFP-targeting
201 shRNA (shGFP). We confirmed that sh*PGBD5*-expressing cells were significantly depleted of
202 *PGBD5* as compared to control shGFP cells (mean fold-depletion = 0.59 and 0.54; t-test $p = 4.7E-$
203 3 and $1.2E-3$, respectively; **Figure 4A**). We then measured DNA damage using quantitative
204 confocal immunofluorescence microscopy of γ H2AX, and found that while the combination of TAZ
205 and elimusertib induced DNA damage in sh*PGBD5* cells, this effect was significantly reduced
206 compared to control shGFP cells (mean fold-reduction = 0.34 and 0.39; t-test $p = 3.9E-8$ and
207 $4.4E-8$ for shGFP versus sh*PGBD5*-1 and sh*PGBD5*-3, respectively; **Figure 4B-C**). This *PGBD5*-
208 dependent reduction in DNA damage was observed both when examining all nuclei with γ H2AX
209 staining (**Figure 4B**), as well as only nuclei with punctate γ H2AX staining, corresponding to more
210 localized DNA damage (mean fold-reduction = 0.59 and 0.61; t-test $p = 2.4E-5$ and $2.7E-5$ for
211 shGFP versus sh*PGBD5*-1 and sh*PGBD5*-3, respectively; **Figure 4D**), as opposed to pan-nuclear
212 γ H2AX staining due to genome-wide unrepaired DNA damage and cellular apoptosis (mean fold-
213 reduction = 0.31 and 0.55; t-test $p = 9.0E-4$ and $1.6E-2$ for shGFP versus sh*PGBD5*-1 and
214 sh*PGBD5*-3, respectively; **Figure 4E**). Thus, *PGBD5* is at least in part necessary for TAZ-
215 mediated induction of DNA damage and its potentiation by the combination with elimusertib.

216

217 This nominates therapeutic targeting of the EZH2-*PGBD5* synthetic lethal dependency as an
218 improved combination strategy for epithelioid and rhabdoid tumors. To test this idea, we
219 assembled a phase 2-like cohort of diverse MRT and ES tumors derived from patients with
220 relapsed and metastatic disease, including tumors with numerous additional acquired mutations
221 (**Supplementary Table S1**). We engrafted these tumors into immunodeficient *NOD-scid*
222 *IL2Rgamma*^{null} mice, and randomized tumor-bearing animals to treatment with TAZ or elimusertib

223 or the combination of both (**Figure 5A**). The combination of TAZ and elimusertib exceeded the
224 effect of treatment with either drug alone when assessed by tumor growth measurements (Vardi
225 *U*-test $p = 2.33E-2$ and 0.20 for combination versus elimusertib or TAZ, respectively; **Figure 5A**)
226 and significantly extended tumor-free survival from 51 days (95% CI = 42-60 days) for elimusertib
227 and 68 days (95% CI = 53-82 days) for TAZ to 100 days (95% CI = 76-124 days) for the
228 combination (log-rank test $p = 5.8E-4$ and $3.8E-2$ for combination versus elimusertib or TAZ,
229 respectively; **Figure 5B**).

230

231 This activity was most pronounced for the HYMAD_EPIS_X0004aS1 and
232 SOMWR_EPIS_X00013aS1 PDX models (**Figures 5C-H**), despite the former exhibiting a
233 relatively poor response to TAZ monotherapy, when assessed by tumor growth measurements
234 (Vardi *U*-test $p = 2.0E-4$ for combination versus elimusertib or TAZ for HYMAD_EPIS_X0003aS1;
235 **Figure 5C**; $p = 1.0E-3$ and $6.0E-2$ for combination versus elimusertib and TAZ, respectively for
236 SOMWR_EPIS_X00013aS1; **Figure 5E**) and tumor-free survival (log-rank test $p = 6.2E-3$ and
237 $6.3E-5$ for combination versus elimusertib or TAZ, respectively for HYMAD_EPIS_X0003aS1;
238 **Figure 5D**; $p = 9.5E-5$ and $6.0E-2$ for combination versus elimusertib or TAZ, respectively for
239 SOMWR_EPIS_X00013aS1; **Figure 5F**). This effect leverages the EZH2-PGBD5 collateral
240 synthetic lethal dependency, targeting PGBD5-dependent DNA damage to improve TAZ clinical
241 response and overcome resistance in epithelioid and rhabdoid tumors.

242

243 Discussion

244

245 Prior studies showed that inhibition of EZH2 methyltransferase activity using tazemetostat is
246 insufficient to induce durable tumor regressions in most patients with epithelioid and rhabdoid
247 tumors (8). Our recent functional genetic studies of patient tumors before and after clinical TAZ
248 therapy led to a specific model of effective epigenetic therapy, including rational combinations to
249 overcome RB1/E2F pathway defects that were observed in 43% of tumors with primary or
250 acquired TAZ resistance (8). Here, we further advanced this approach by identifying a collateral
251 synthetic lethal dependency between EZH2 and PGBD5 in rhabdoid and epithelioid sarcomas
252 that confers a susceptibility to combined epigenetic therapy using EZH2 and ATR inhibition. We
253 found that EZH2 inhibition can upregulate the transposase-derived PGBD5 nuclease, which
254 induces DNA damage, requiring ATR but not CHK1-mediated DNA damage repair signaling in
255 *SMARCB1*-deficient rhabdoid and epithelioid tumors regardless of their *RB1* mutational status.
256 As a result, combined EZH2 and ATR inhibition exerts synergistic anti-tumor effects, as measured

257 by DNA damage induction *in vitro* and tumor growth reduction and improvements in tumor-free
258 survival *in vivo*.

259

260 The combination of EZH2 and ATR inhibition offers both a promising therapeutic approach that
261 can be rapidly translated to clinical trials for patients with rhabdoid and epithelioid sarcomas,
262 and a compelling example of drug-induced synthetic lethality. Originally described as genetic
263 interactions (21), synthetic lethal targeting has proven to be a powerful therapeutic approach for
264 the treatment of cancers. For example, breast and ovarian carcinomas with *BRCA1/2* mutations
265 exhibit increased dependence on poly(adenosine diphosphate-ribose) polymerase (PARP)-
266 mediated DNA repair, conferring a susceptibility to PARP1/2 inhibitors such as olaparib (22, 23).
267 Synthetic dependencies in DNA damage signaling, chromatin remodeling, and metabolic
268 functions have recently been defined to develop improved targeted therapies (24-28). In
269 particular, acquired defects in DNA repair in tumor cells, such as inactivating mutations or
270 functional defects in ATM signaling, can confer susceptibility to ATR inhibition due to the
271 specific requirements of concurrent ATM and ATR signaling for efficient NHEJ DNA repair and
272 tumor cell survival (28-32).

273

274 ATR-selective inhibitors also synergize with genotoxic chemotherapies, such as DNA cross-
275 linking platinum drugs, due to the specific requirements of ATR-dependent DNA repair during
276 DNA replication (28). However, this approach has limited therapeutic efficacy due to its effects
277 on healthy cells. Thus, effective targeting of DNA damage repair must leverage tumor-specific
278 mutational and repair processes, providing a rationale for combining epigenetic and DNA repair
279 inhibitors. In the case of rhabdoid and epithelioid sarcomas with *SMARCB1* deficiency, the
280 epigenetic antagonism between the chromatin remodeling activities of BAF and PRC2
281 contributes to the dependency of tumor cells on EZH2 activity (5), whose inhibition promotes the
282 expression of tumor suppressors otherwise repressed by PRC2 (8, 33). This epigenetic
283 reprogramming also appears to increase the expression of *PGBD5*, with the associated DNA
284 damage and requirement for its ATR-dependent repair. It remains to be defined whether this
285 effect is due to direct repression through PRC2-mediated histone 3 lysine 27 trimethylation of
286 the *PGBD5* locus and/or indirect transcriptional or post-transcriptional regulation of *PGBD5*
287 expression.

288

289 Though the cell of origin of rhabdoid and epithelioid sarcomas is currently unknown, these tumors
290 exhibit epigenetic and transcriptional features of neuronal and neural crest cells (34-36). EZH2 is

291 known to regulate neuronal differentiation (37-40), and therefore it will also be important to
292 determine whether EZH2 inhibition of other PGBD5-expressing tumors, such as neuroblastomas,
293 medulloblastomas, and Ewing and other fusion sarcomas, all of which also share features of
294 neuronal lineages, can also induce PGBD5-dependent DNA damage, thereby conferring a
295 susceptibility to collateral synthetic lethal targeting with ATR inhibitors. Importantly, susceptibility
296 to ATR inhibition can also result from PGBD5-independent sources of intrinsic DNA damage, such
297 as alternative lengthening of telomeres (ALT) (41), replication stress due to transcriptional-
298 replication interference (42-44), and functional ATM defects (30, 45), all of which may occur
299 concurrently in tumor cells undergoing PGBD5-dependent DNA damage. Similarly, EZH2 may
300 also contribute to other mechanisms of DNA damage repair (46-53). Thus, future biochemical and
301 genetic studies will be needed to define specific mechanisms of EZH2 and ATR-dependent DNA
302 damage repair signaling in tumor and healthy cells to identify improved targets to develop
303 exclusively tumor-selective therapies. This direction is particularly compelling because PGBD5-
304 dependent DNA damage repair appears to require ATR but not CHK1 kinase signaling in
305 epithelioid and rhabdoid tumor cells, in contrast to ATR/CHK1-dependent canonical signaling
306 observed during replication stress in healthy tissues.

307
308 Further definition of the EZH2-PGBD5 collateral synthetic lethal mechanisms should also aid in
309 therapy stratification of combined EZH2 and ATR inhibition. For example, apparent variation in
310 response to the tazemetostat-elimusertib combination between patient-derived epithelioid and
311 rhabdoid tumors may result from biological differences in DNA damage repair signaling, PGBD5
312 activity, or other sources of intrinsic DNA damage, which in turn may be associated with the
313 recently described distinct molecular subtypes of ES and MRT tumors (54). In addition, both
314 EZH2 and ATR inhibition can be immunogenic (8, 55-57), and future studies will be needed to
315 define immunologic effects of this combination therapy that may contribute to therapeutic effects
316 in patients. In all, this work emphasizes how improved understanding of collateral dependencies
317 of intrinsic mutators and epigenetic dysregulation responsible for causing childhood and young-
318 onset cancers can be leveraged for rational combination therapies.

319

320 **Acknowledgements**

321

322 This work is dedicated to Maggie Schmidt and her family, and to the many other patients and
323 their advocates who inspire and support our research. We thank Richard Koche, Nicholas
324 Succi, and Mithat Gönen for technical advice, Marc Ladanyi for patient-derived xenografts,

325 members of our labs for critical advice and manuscript comments, and Epizyme (now Ipsen)
326 and Bayer for supplying tazemetostat and elimusertib, respectively. This work was supported by
327 the MSK Integrated Genomics Operation Core, Anti-Tumor Assessment Core, Bioinformatics
328 Core, Molecular Diagnostics Service and the Department of Pathology, the Marie-Josée and
329 Henry R. Kravis Center for Molecular Oncology, NIH R01 CA214812, P30 CA08748, T32
330 GM007739, Burroughs Wellcome Fund, Rita Allen Foundation, Pershing Square Sohn Cancer
331 Research Alliance and the G. Harold and Leila Y. Mathers Foundation, Cycle for Survival, MSK
332 Sarcoma Center, the Starr Cancer Consortium, and Maggie's Mission. Yaniv Kazansky was
333 supported by a Medical Scientist Training Program grant from the National Institute of General
334 Medical Sciences of the National Institutes of Health under award number T32 GM007739 to
335 the Weill Cornell/Rockefeller/Sloan Kettering Tri-Institutional MD-PhD Program. AK is a Scholar
336 of the Leukemia & Lymphoma Society.

337

338

339 **Methods**

340

341 Cell culture

342 G401, TTC642, VAESBJ, and TM8716 cell lines were obtained from the American Type Culture
343 Collection. The ES1 cell line was generated and kindly provided by Nadia Zaffaroni. Rhabdoid
344 tumor cell lines KP-MRT-NS and KP-MRT-RY were kindly provided by Yasumichi Kuwahara and
345 Hajime Hosoi. The identity of all cell lines was verified by STR analysis. Absence of *Mycoplasma*
346 contamination was determined at every plating using the MycoAlert kit according to
347 manufacturer's instructions (Lonza). Cell lines were cultured in 5% CO₂ in a humidified
348 atmosphere in 37°C. All media were obtained from Corning and supplemented with 10% fetal
349 bovine serum (FBS), 1% L-glutamine, and 100 U/mL penicillin and 100 µg/mL streptomycin
350 (Gibco). G401, ES1, and VAESBJ cells were cultured in Dulbecco's Modified Eagle Medium
351 (DMEM). TTC642, TM8716, KP-MRT-NS, and KP-MRT-RY cells were cultured in Roswell Park
352 Memorial Institute (RPMI) medium. All experiments were performed using cell lines kept in culture
353 for no more than 10 passages. Generation of G401 with *RB1* deletion was described previously
354 (8) using the gRNA sequence in Table 1 below.

355

356 Western blotting

357 To assess protein expression by Western immunoblotting, pellets of 1 million cells were prepared
358 and washed once in cold PBS. Cells were resuspended in 100-130 µL of RIPA lysis buffer (50
359 mM Tris-HCl, pH 8.0, 150 mM NaCl, 1.0% NP-40, 0.5% sodium deoxycholate, 0.1% sodium

360 dodecyl sulfate) and incubated on ice for 10 minutes. Cell suspensions were then disrupted using
361 a Covaris S220 adaptive focused sonicator for 5 minutes (peak incident power: 35W, duty factor:
362 10%, 200 cycles/burst) at 4 °C. Lysates were cleared by centrifugation at 18,000 g for 15 min at
363 4 °C. Protein concentration was assayed using the DC Protein Assay (Bio-Rad) and 15-35 µg
364 whole cell extract was used per sample. Samples were boiled at 95 °C in Laemmli buffer (Bio-
365 Rad) with 40 mM DTT and resolved using sodium dodecyl sulfate-polyacrylamide gel
366 electrophoresis. Proteins were transferred to Immobilon FL PVDF membranes (Millipore), and
367 membranes were blocked using Intercept Blocking buffer (Li-Cor). Primary antibodies used were:
368 anti-EZH2 (Cell Signaling Technology, 5246) at 1:1,000, anti-RPA32 pT21 (abcam, ab109394) at
369 1:2,000, anti-RPA32 pS4/pS8 (ThermoFisher, A300-245A) at 1:2,000, anti-pCHK1 S296 (Cell
370 Signaling Technology, 90178) at 1:250, anti-MYCN (Cell Signaling Technology, 9405) at 1:250,
371 anti-Actin (Cell Signaling Technology, 4970 and 3700) at 1:5,000. Blotted membranes were
372 visualized using goat secondary antibodies conjugated to IRDye 680RD or IRDye 800CW (Li-
373 Cor, 926-68071 and 926-32210) at 1:15,000 and the Odyssey CLx fluorescence scanner,
374 according to manufacturer's instructions (Li-Cor). Image analysis was done using the Li-Cor
375 Image Studio software (version 4).

376

377 Transcriptomic data

378 Expression levels of *PGBD5* and *MYCN* in G401 cells were determined from our previously
379 published dataset (8). Transcriptomic data and metaVIPER protein activity inference was
380 performed as previously described (15, 16).

381

382 Generating shPGBD5 cells

383 For shRNA cells, pLKO.1 shRNA vectors targeting *PGBD5* (TRCN0000138412,
384 TRCN0000135121) and control shGFP were obtained from the RNAi Consortium (Broad
385 Institute). Lentivirus production was carried out as described previously (8). G401 cells were
386 transduced at an MOI ~1.5 and selected with puromycin at 2 µg/mL for 72 hours. Knockdown was
387 confirmed by quantitative RT-PCR as previously described (9), using primers specified in the
388 Table 1.

389

390 Combination drug treatment

391 Drugs used for *in vitro* treatment were supplied by Selleckchem (TAZ, S7128; Elimusertib, S9864;
392 camptothecin, S1288; SRA737, S8253).

393

394 For combination treatment with TAZ and elimusertib, we used a two-dimensional dose matrix
395 design, treating the cells for 9 days. After the addition of cells, drugs were added using a pin tool
396 (stainless steel pins with 50 nL slots, V&P Scientific) mounted onto a liquid handling robot (CyBio
397 Well vario, Analytik Jena). On Day 9, CellTiter-Glo reagent was freshly reconstituted and added
398 in a 1:1 proportion to cell media, according to the manufacturer's instructions. A similar protocol
399 was used for monotherapy dose response curves for elimusertib and SRA737, although drug
400 solutions were added manually, and specific treatment times are indicated in the corresponding
401 figure legends. For analysis of synergy, we used the synergyFinder package (58). Outliers due to
402 pinning errors were excluded after manual examination.

403

404 Immunofluorescence

405 Immunofluorescence for γ H2AX was performed on cells plated on Millicell EZ Slide glass slides
406 (EMD Millipore), coated for 45 minutes with bovine plasma fibronectin (Millipore Sigma). After
407 drug treatment, cells were washed once with PBS and fixed in 4% formaldehyde for 10 minutes
408 at room temperature. Slides were then washed three times in PBS for 5 minutes, permeabilized
409 for 15 minutes in 0.3% Triton X-100, washed again in PBS three times, and blocked with 5%
410 goat serum (Millipore Sigma, G9023) in PBS for 1 hour at room temperature. Slides were
411 incubated with mouse anti- γ H2A.X primary antibody (Sigma-Aldrich, 05-636) at 1:500 in
412 blocking buffer for 1 hour, washed three times in PBS, and incubated with goat anti-mouse
413 secondary antibody conjugated to AlexaFluor555 (Invitrogen, A-21422) at 1:1,000. Cells were
414 then counterstained with DAPI at 1:1,000 for 10 minutes and treated with ProLong Diamond
415 Antifade Mountant with DAPI (Invitrogen, P36962) for 48 hours.

416

417 Images were acquired on a Zeiss LSM880 confocal microscope at 63x magnification. Images
418 were then processed using a custom pipeline in CellProfiler (59). Per-cell integrated γ H2A.X
419 intensity was normalized against per-cell integrated DAPI intensity. All image analysis used the
420 same pipeline settings, with the exception of the RescaleIntensity module for the AF555
421 channel, which used the settings 0.009-0.09 for the images in Figure 2 and 0.005-0.09 for
422 Figure 4. CellProfiler analysis pipeline files and raw image files are available on Zenodo (DOI:
423 10.5281/zenodo.10982946). Overlaid images were prepared using Fiji (60).

424

425 Xenografts

426 All mouse experiments were carried out in accordance with institutionally approved animal use
427 protocols (8). To generate PDXs, tumor specimens were collected under approved IRB protocol

428 14-091, immediately minced and mixed (50:50) with Matrigel (Corning, New York, NY) and
429 implanted subcutaneously in the flank of 6-8 weeks-old female NOD.Cg-*Prkdc*^{scid} *Il2rg*^{tm1Wjl}/Sjz
430 (NSG) mice (Jackson Laboratory, Bar Harbor, ME), as described previously (61). Mice were
431 monitored daily and PDX samples were serially transplanted three times before being deemed
432 established. PDX tumor histology was confirmed by review of H&E slides and direct comparison
433 to the corresponding patient tumor slides. PDX identity was further confirmed by MSK-IMPACT
434 sequencing analysis.

435

436 Therapeutic studies used female and male NSG mice obtained from the Jackson Laboratory.
437 Xenografts were prepared as single-cell suspensions, resuspended in Matrigel, and implanted
438 subcutaneously into the right flank of 6-10 week old mice. 100 μ L of tumor cell suspension was
439 used for each mouse. Tumors were allowed to grow until they reached a volume of 100 mm³, at
440 which point they were randomized into treatment groups without blinding. Drugs were prepared
441 using the following formulations: Tazemetostat was dissolved at 25 mg/mL in 5% DMSO, 40%
442 PEG 300, 5% Tween 80, and 50% water. Elimusertib was dissolved at 5 mg/mL in 10% DMSO,
443 40% PEG 300, 5% Tween 80, and 45% water using a sonicator. Drugs were reconstituted daily.
444 TAZ was dosed at 250 mg/kg twice daily by oral gavage, 7 days per week. Elimusertib was
445 dosed at 40 mg/kg twice daily by oral gavage using 2 days on and 12 days off cycle. Caliper
446 tumor measurements were taken twice weekly. Tumor volumes were calculated using the
447 formula $\text{Volume} = (\pi/6) \times \text{length} \times \text{width}^2$. Tumor growth analysis was performed using the Vardi
448 *U*-test (62), as implemented in the clinfun R package using the aucVardiTest function. Tumor-
449 free survival analysis was calculated using OriginPro (Microcal) by the Kaplan-Meier method,
450 using the log-rank test. Raw data and R scripts used for data analysis are available on Zenodo
451 (DOI: 10.5281/zenodo.10398544).

452

453 **Supplementary Table S1:** List of PDX models used in this study, with clinical characteristics of
454 the original tumor specimens, followed by a list of mutations found in all PDX models, as
455 determined by targeted MSK-IMPACT sequencing.

456

457

458

459

460

461

462

463

464

465 References

- 466 1. Kadoch C, Crabtree GR. Mammalian SWI/SNF chromatin remodeling complexes and cancer:
467 Mechanistic insights gained from human genomics. *Sci Adv.* 2015;1(5):e1500447.
- 468 2. Versteeg I, Sévenet N, Lange J, Rousseau-Merck MF, Ambros P, Handgretinger R, et al.
469 Truncating mutations of hSNF5/INI1 in aggressive paediatric cancer. *Nature.*
470 1998;394(6689):203-6.
- 471 3. Kim KH, Kim W, Howard TP, Vazquez F, Tsherniak A, Wu JN, et al. SWI/SNF-mutant
472 cancers depend on catalytic and non-catalytic activity of EZH2. *Nat Med.* 2015;21(12):1491-6.
- 473 4. McKenna ES, Sansam CG, Cho YJ, Greulich H, Evans JA, Thom CS, et al. Loss of the
474 epigenetic tumor suppressor SNF5 leads to cancer without genomic instability. *Mol Cell Biol.*
475 2008;28(20):6223-33.
- 476 5. Wilson BG, Wang X, Shen X, McKenna ES, Lemieux ME, Cho YJ, et al. Epigenetic
477 antagonism between polycomb and SWI/SNF complexes during oncogenic transformation.
478 *Cancer Cell.* 2010;18(4):316-28.
- 479 6. Kadoch C, Williams RT, Calarco JP, Miller EL, Weber CM, Braun SM, et al. Dynamics of
480 BAF-Polycomb complex opposition on heterochromatin in normal and oncogenic states. *Nat*
481 *Genet.* 2017;49(2):213-22.
- 482 7. Gounder M, Schöffski P, Jones RL, Agulnik M, Cote GM, Villalobos VM, et al. Tazemetostat
483 in advanced epithelioid sarcoma with loss of INI1/SMARCB1: an international, open-label,
484 phase 2 basket study. *Lancet Oncol.* 2020;21(11):1423-32.
- 485 8. Kazansky Y, Cameron D, Mueller HS, Demarest P, Zaffaroni N, Arrighetti N, et al.
486 Overcoming clinical resistance to EZH2 inhibition using rational epigenetic combination therapy.
487 *Cancer Discov.* 2024.
- 488 9. Henssen AG, Koche R, Zhuang J, Jiang E, Reed C, Eisenberg A, et al. PGBD5 promotes
489 site-specific oncogenic mutations in human tumors. *Nat Genet.* 2017;49(7):1005-14.
- 490 10. Biegel JA, Zhou JY, Rorke LB, Stenstrom C, Wainwright LM, Fogelgren B. Germ-line and
491 acquired mutations of INI1 in atypical teratoid and rhabdoid tumors. *Cancer Res.* 1999;59(1):74-
492 9.
- 493 11. Chun HE, Johann PD, Milne K, Zapatka M, Buellesbach A, Ishaque N, et al. Identification
494 and Analyses of Extra-Cranial and Cranial Rhabdoid Tumor Molecular Subgroups Reveal
495 Tumors with Cytotoxic T Cell Infiltration. *Cell Rep.* 2019;29(8):2338-54.e7.
- 496 12. Henssen AG, Henaff E, Jiang E, Eisenberg AR, Carson JR, Villasante CM, et al. Genomic
497 DNA transposition induced by human PGBD5. *Elife.* 2015;4.
- 498 13. Yamada M, Keller RR, Gutierrez RL, Cameron D, Suzuki H, Sanghrajka R, et al. Childhood
499 cancer mutagenesis caused by transposase-derived PGBD5. *Sci Adv.* 2024;10(12):eadn4649.
- 500 14. Henssen AG, Reed C, Jiang E, Garcia HD, von Stebut J, MacArthur IC, et al. Therapeutic
501 targeting of PGBD5-induced DNA repair dependency in pediatric solid tumors. *Sci Transl Med.*
502 2017;9(414).
- 503 15. Ding H, Douglass EF, Jr., Sonabend AM, Mela A, Bose S, Gonzalez C, et al. Quantitative
504 assessment of protein activity in orphan tissues and single cells using the metaVIPER
505 algorithm. *Nat Commun.* 2018;9(1):1471.
- 506 16. Coutinho DF, Mundi PS, Marks LJ, Burke C, Ortiz MV, Diolaiti D, et al. Validation of a non-
507 oncogene encoded vulnerability to exportin 1 inhibition in pediatric renal tumors. *Med.*
508 2022;3(11):774-91.e7.
- 509 17. Mundi PS, Dela Cruz FS, Grunn A, Diolaiti D, Mauguen A, Rainey AR, et al. A
510 Transcriptome-Based Precision Oncology Platform for Patient–Therapy Alignment in a Diverse
511 Set of Treatment-Resistant Malignancies. *Cancer Discovery.* 2023;13(6):1386-407.
- 512 18. Lee CY, The M, Meng C, Bayer FP, Putzker K, Müller J, et al. Illuminating phenotypic drug
513 responses of sarcoma cells to kinase inhibitors by phosphoproteomics. *Mol Syst Biol.*
514 2024;20(1):28-55.

- 515 19. León TE, Rapoz-D'Silva T, Bertoli C, Rahman S, Magnussen M, Philip B, et al. EZH2-
516 Deficient T-cell Acute Lymphoblastic Leukemia Is Sensitized to CHK1 Inhibition through
517 Enhanced Replication Stress. *Cancer Discov.* 2020;10(7):998-1017.
- 518 20. Ngoi NYL, Pilié PG, McGrail DJ, Zimmermann M, Schlacher K, Yap TA. Targeting ATR in
519 patients with cancer. *Nature Reviews Clinical Oncology.* 2024;21(4):278-93.
- 520 21. Dobzhansky T. Genetics of natural populations; recombination and variability in populations
521 of *Drosophila pseudoobscura*. *Genetics.* 1946;31(3):269-90.
- 522 22. Farmer H, McCabe N, Lord CJ, Tutt AN, Johnson DA, Richardson TB, et al. Targeting the
523 DNA repair defect in BRCA mutant cells as a therapeutic strategy. *Nature.* 2005;434(7035):917-
524 21.
- 525 23. Bryant HE, Schultz N, Thomas HD, Parker KM, Flower D, Lopez E, et al. Specific killing of
526 BRCA2-deficient tumours with inhibitors of poly(ADP-ribose) polymerase. *Nature.*
527 2005;434(7035):913-7.
- 528 24. Muller FL, Colla S, Aquilanti E, Manzo VE, Genovese G, Lee J, et al. Passenger deletions
529 generate therapeutic vulnerabilities in cancer. *Nature.* 2012;488(7411):337-42.
- 530 25. Zhao D, Lu X, Wang G, Lan Z, Liao W, Li J, et al. Synthetic essentiality of chromatin
531 remodelling factor CHD1 in PTEN-deficient cancer. *Nature.* 2017;542(7642):484-8.
- 532 26. Kwok M, Davies N, Agathangelou A, Smith E, Petermann E, Yates E, et al. Synthetic
533 lethality in chronic lymphocytic leukaemia with DNA damage response defects by targeting the
534 ATR pathway. *Lancet.* 2015;385 Suppl 1:S58.
- 535 27. Toledo LI, Murga M, Zur R, Soria R, Rodriguez A, Martinez S, et al. A cell-based screen
536 identifies ATR inhibitors with synthetic lethal properties for cancer-associated mutations. *Nat*
537 *Struct Mol Biol.* 2011;18(6):721-7.
- 538 28. Reaper PM, Griffiths MR, Long JM, Charrier JD, Maccormick S, Charlton PA, et al. Selective
539 killing of ATM- or p53-deficient cancer cells through inhibition of ATR. *Nat Chem Biol.*
540 2011;7(7):428-30.
- 541 29. Middleton FK, Patterson MJ, Elstob CJ, Fordham S, Herriott A, Wade MA, et al. Common
542 cancer-associated imbalances in the DNA damage response confer sensitivity to single agent
543 ATR inhibition. *Oncotarget.* 2015;6(32):32396-409.
- 544 30. Shruti M, Marcus RB, Yone Phar L, Hannah A, Shruthi P, Ann H, et al. FET fusion
545 oncoproteins disrupt physiologic DNA repair networks in cancer. *bioRxiv.*
546 2023:2023.04.30.538578.
- 547 31. Min A, Im SA, Jang H, Kim S, Lee M, Kim DK, et al. AZD6738, A Novel Oral Inhibitor of
548 ATR, Induces Synthetic Lethality with ATM Deficiency in Gastric Cancer Cells. *Mol Cancer*
549 *Ther.* 2017;16(4):566-77.
- 550 32. Menezes DL, Holt J, Tang Y, Feng J, Barsanti P, Pan Y, et al. A synthetic lethal screen
551 reveals enhanced sensitivity to ATR inhibitor treatment in mantle cell lymphoma with ATM loss-
552 of-function. *Mol Cancer Res.* 2015;13(1):120-9.
- 553 33. Knutson SK, Warholic NM, Wigle TJ, Klaus CR, Allain CJ, Raimondi A, et al. Durable tumor
554 regression in genetically altered malignant rhabdoid tumors by inhibition of methyltransferase
555 EZH2. *Proc Natl Acad Sci U S A.* 2013;110(19):7922-7.
- 556 34. Gadd S, Sredni ST, Huang C-C, Perlman EJ. Rhabdoid tumor: gene expression clues to
557 pathogenesis and potential therapeutic targets. *Laboratory Investigation.* 2010;90(5):724-38.
- 558 35. Custers L, Khabirova E, Coorens THH, Oliver TRW, Calandrini C, Young MD, et al. Somatic
559 mutations and single-cell transcriptomes reveal the root of malignant rhabdoid tumours. *Nat*
560 *Commun.* 2021;12(1):1407.
- 561 36. Chun HE, Lim EL, Heravi-Moussavi A, Saberi S, Mungall KL, Bilenky M, et al. Genome-
562 Wide Profiles of Extra-cranial Malignant Rhabdoid Tumors Reveal Heterogeneity and
563 Dysregulated Developmental Pathways. *Cancer Cell.* 2016;29(3):394-406.

- 564 37. Pereira JD, Sansom SN, Smith J, Dobenecker MW, Tarakhovskiy A, Livesey FJ. Ezh2, the
565 histone methyltransferase of PRC2, regulates the balance between self-renewal and
566 differentiation in the cerebral cortex. *Proc Natl Acad Sci U S A*. 2010;107(36):15957-62.
- 567 38. Zhang J, Ji F, Liu Y, Lei X, Li H, Ji G, et al. Ezh2 regulates adult hippocampal neurogenesis
568 and memory. *J Neurosci*. 2014;34(15):5184-99.
- 569 39. Di Meglio T, Kratochwil CF, Vilain N, Loche A, Vitobello A, Yonehara K, et al. Ezh2
570 orchestrates topographic migration and connectivity of mouse precerebellar neurons. *Science*.
571 2013;339(6116):204-7.
- 572 40. Zhang M, Zhang Y, Xu Q, Crawford J, Qian C, Wang GH, et al. Neuronal Histone
573 Methyltransferase EZH2 Regulates Neuronal Morphogenesis, Synaptic Plasticity, and Cognitive
574 Behavior in Mice. *Neurosci Bull*. 2023;39(10):1512-32.
- 575 41. Flynn RL, Cox KE, Jeitany M, Wakimoto H, Bryll AR, Ganem NJ, et al. Alternative
576 lengthening of telomeres renders cancer cells hypersensitive to ATR inhibitors. *Science*.
577 2015;347(6219):273-7.
- 578 42. Dorado García H, Pusch F, Bei Y, von Stebut J, Ibáñez G, Guillan K, et al. Therapeutic
579 targeting of ATR in alveolar rhabdomyosarcoma. *Nat Commun*. 2022;13(1):4297.
- 580 43. Zeman MK, Cimprich KA. Causes and consequences of replication stress. *Nat Cell Biol*.
581 2014;16(1):2-9.
- 582 44. Schoppy DW, Ragland RL, Gilad O, Shastri N, Peters AA, Murga M, et al. Oncogenic stress
583 sensitizes murine cancers to hypomorphic suppression of ATR. *J Clin Invest*. 2012;122(1):241-
584 52.
- 585 45. Kwok M, Davies N, Agathangelou A, Smith E, Oldreive C, Petermann E, et al. ATR
586 inhibition induces synthetic lethality and overcomes chemoresistance in TP53- or ATM-defective
587 chronic lymphocytic leukemia cells. *Blood*. 2016;127(5):582-95.
- 588 46. Karakashev S, Fukumoto T, Zhao B, Lin J, Wu S, Fatkhutdinov N, et al. EZH2 Inhibition
589 Sensitizes CARM1-High, Homologous Recombination Proficient Ovarian Cancers to PARP
590 Inhibition. *Cancer Cell*. 2020;37(2):157-67.e6.
- 591 47. Zhang X, Huo X, Guo H, Xue L. Combined inhibition of PARP and EZH2 for cancer
592 treatment: Current status, opportunities, and challenges. *Front Pharmacol*. 2022;13:965244.
- 593 48. Ratz L, Brambillasca C, Bartke L, Huetzen MA, Goergens J, Leidecker O, et al. Combined
594 inhibition of EZH2 and ATM is synthetic lethal in BRCA1-deficient breast cancer. *Breast Cancer*
595 *Res*. 2022;24(1):41.
- 596 49. Campbell S, Ismail IH, Young LC, Poirier GG, Hendzel MJ. Polycomb repressive complex 2
597 contributes to DNA double-strand break repair. *Cell Cycle*. 2013;12(16):2675-83.
- 598 50. Chou DM, Adamson B, Dephore NE, Tan X, Nottke AC, Hurov KE, et al. A chromatin
599 localization screen reveals poly (ADP ribose)-regulated recruitment of the repressive polycomb
600 and NuRD complexes to sites of DNA damage. *Proc Natl Acad Sci U S A*. 2010;107(43):18475-
601 80.
- 602 51. Ito T, Teo YV, Evans SA, Neretti N, Sedivy JM. Regulation of Cellular Senescence by
603 Polycomb Chromatin Modifiers through Distinct DNA Damage- and Histone Methylation-
604 Dependent Pathways. *Cell Rep*. 2018;22(13):3480-92.
- 605 52. Piunti A, Rossi A, Cerutti A, Albert M, Jammula S, Scelfo A, et al. Polycomb proteins control
606 proliferation and transformation independently of cell cycle checkpoints by regulating DNA
607 replication. *Nat Commun*. 2014;5:3649.
- 608 53. Rondinelli B, Gogola E, Yücel H, Duarte AA, van de Ven M, van der Sluijs R, et al. EZH2
609 promotes degradation of stalled replication forks by recruiting MUS81 through histone H3
610 trimethylation. *Nat Cell Biol*. 2017;19(11):1371-8.
- 611 54. Pinto EM, Hamideh D, Bahrami A, Orr BA, Lin T, Pounds S, et al. Malignant rhabdoid
612 tumors originating within and outside the central nervous system are clinically and molecularly
613 heterogeneous. *Acta Neuropathol*. 2018;136(2):315-26.

- 614 55. Burr ML, Sparbier CE, Chan KL, Chan YC, Kersbergen A, Lam EYN, et al. An Evolutionarily
615 Conserved Function of Polycomb Silences the MHC Class I Antigen Presentation Pathway and
616 Enables Immune Evasion in Cancer. *Cancer Cell*. 2019;36(4):385-401.e8.
- 617 56. Mehdipour P, Marhon SA, Ettayebi I, Chakravarthy A, Hosseini A, Wang Y, et al. Epigenetic
618 therapy induces transcription of inverted SINEs and ADAR1 dependency. *Nature*.
619 2020;588(7836):169-73.
- 620 57. Ishak CA, Marshall AE, Passos DT, White CR, Kim SJ, Cecchini MJ, et al. An RB-EZH2
621 Complex Mediates Silencing of Repetitive DNA Sequences. *Mol Cell*. 2016;64(6):1074-87.
- 622 58. Ianevski A, Giri AK, Aittokallio T. SynergyFinder 2.0: visual analytics of multi-drug
623 combination synergies. *Nucleic Acids Res*. 2020;48(W1):W488-w93.
- 624 59. Stirling DR, Swain-Bowden MJ, Lucas AM, Carpenter AE, Cimini BA, Goodman A.
625 CellProfiler 4: improvements in speed, utility and usability. *BMC Bioinformatics*. 2021;22(1):433.
- 626 60. Schindelin J, Arganda-Carreras I, Frise E, Kaynig V, Longair M, Pietzsch T, et al. Fiji: an
627 open-source platform for biological-image analysis. *Nat Methods*. 2012;9(7):676-82.
- 628 61. Mattar M, McCarthy CR, Kulick AR, Qeriqi B, Guzman S, de Stanchina E. Establishing and
629 Maintaining an Extensive Library of Patient-Derived Xenograft Models. *Front Oncol*. 2018;8:19.
- 630 62. Vardi Y, Ying Z, Zhang CH. Two-sample tests for growth curves under dependent right
631 censoring. *Biometrika*. 2001;88(4):949-60.

632

633

634

635

636

637

638

639

640

641

642

643

644

645

646

647

648

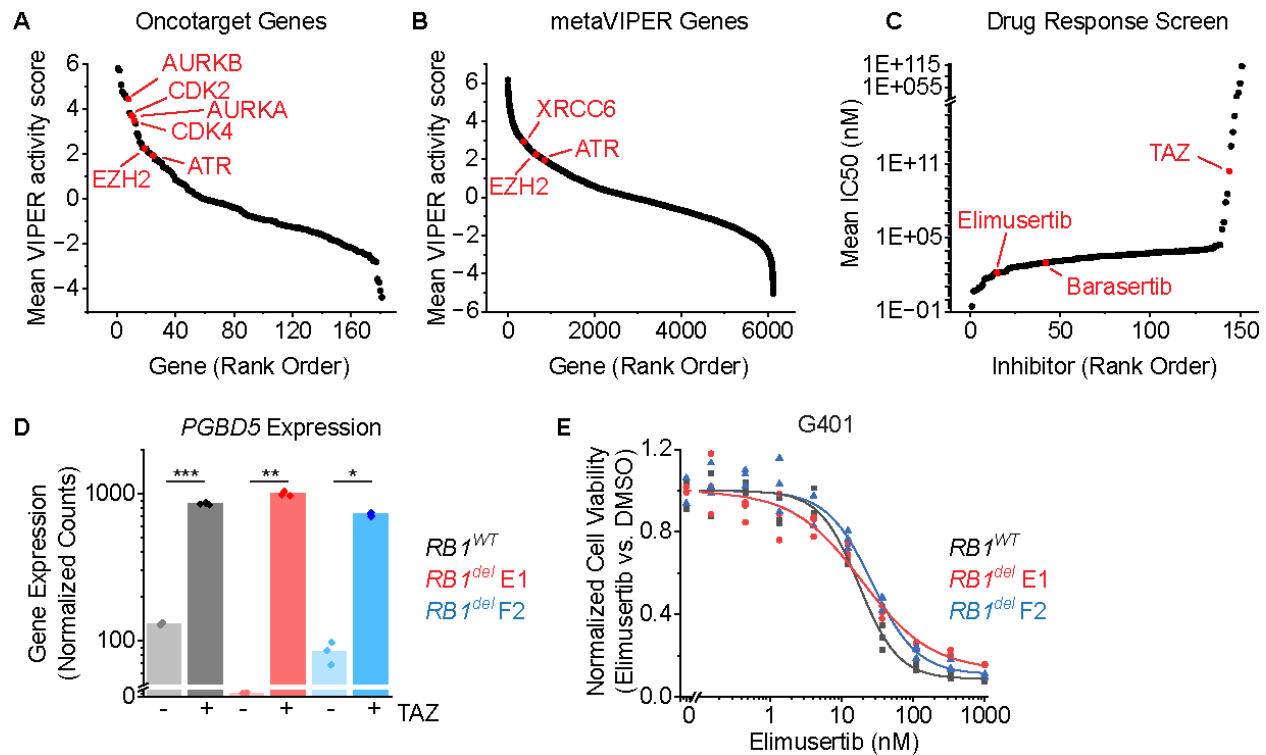
649

650

651 **Table 1:** List of oligonucleotides

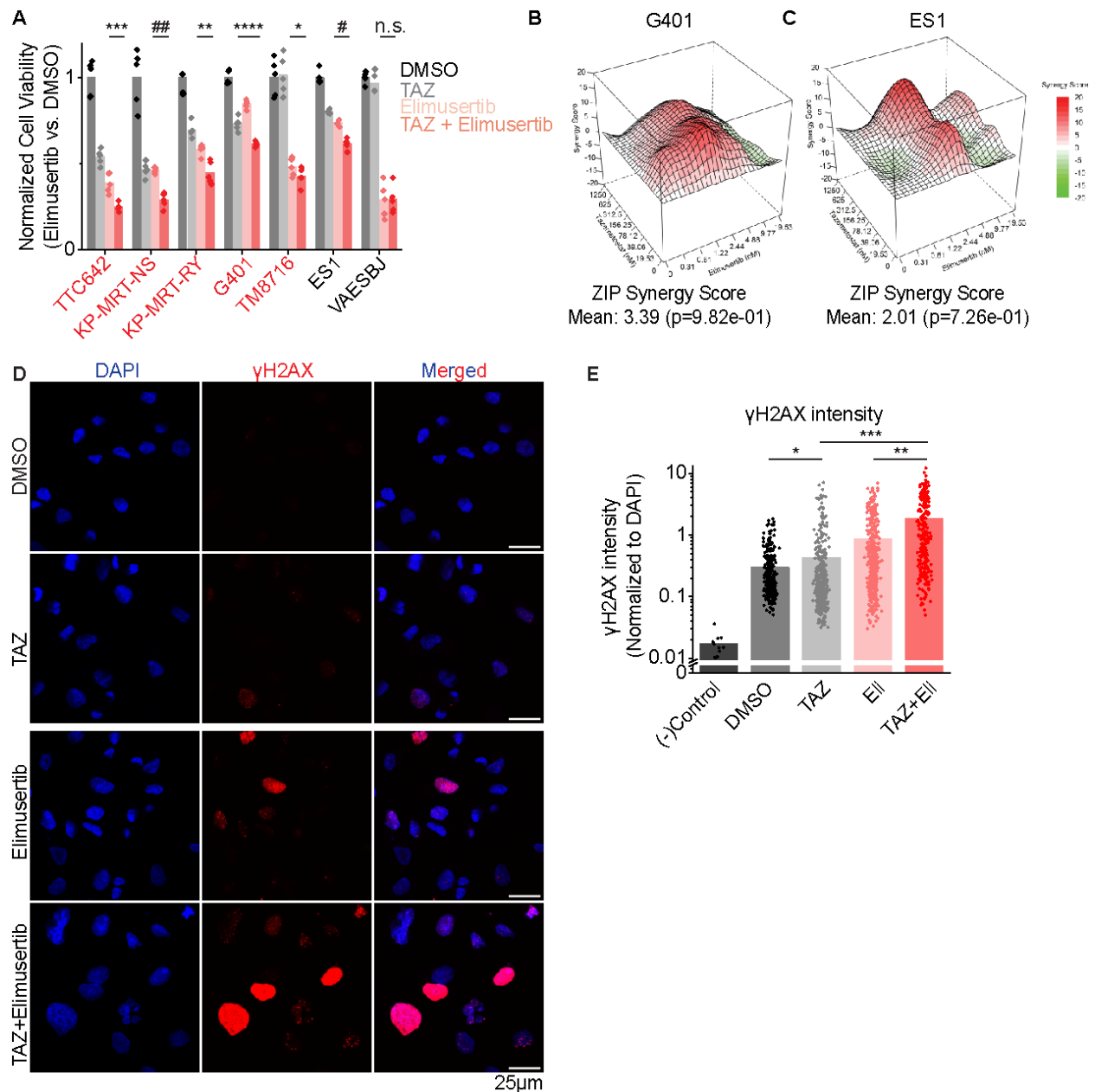
gRNAs	
<i>RB1</i> crRNA	5'- AGAGAGAGCUUGGUUAACUU -3'
Primers for amplification	
<i>PGBD5</i> forward	5'- CTCTGGGTCAGACAATGTTCTTC -3'
<i>PGBD5</i> reverse	5'- GCTTATTCTTCAGCGCATCCA -3'
<i>GAPDH</i> forward	5'- GATCATCAGCAATGCCTCCT -3'
<i>GAPDH</i> reverse	5'- GTCATGAGTCCTTCCACGATAC -3'

652
653
654
655
656
657
658
659
660
661
662
663
664



665
 666
 667
 668
 669
 670
 671
 672
 673
 674
 675
 676
 677
 678
 679
 680
 681
 682
 683
 684
 685
 686
 687
 688
 689
 690
 691

Figure 1: ATR inhibition is a compelling therapeutic target and overcomes TAZ resistance in rhabdoid tumors: (A-B) metaVIPER analysis of rhabdoid tumor transcriptomes for proteins within OncoTarget (A) and the complete metaVIPER protein set (B). (C) Inhibitors rank-ordered by IC50 from Kuster et al. (D) DESeq2-normalized read counts of cells treated with 10 μ M TAZ versus equivalent volume of DMSO for 11 days. n=3 biological replicates per condition. * $p = 1.6E-6$, ** $p = 1.3E-6$, *** $p = 1.2E-7$ by two-sided Student's t-test. (E) G401 cells treated with elimusertib for 4 days.



692

693

694 **Figure 2: Combination EZH2 and ATR inhibition improves response in vitro:** (A) Panel of

695 MRT and ES cell lines ordered left to right by decreasing response to TAZ monotherapy. Cells

696 were treated with the indicated monotherapy or combination for 11 days. Drug concentrations

697 used were: TAZ: 200 nM, elimusertib: 8 nM. We selected an elimusertib dose below its

698 monotherapy IC₅₀ (for G401 cells) in order to visualize any additive effects upon combination with

699 TAZ. **p* = 0.14, ***p* = 3.3E-3, ****p* = 1.0E-3, *****p* = 2.6E-4, #*p* = 6.1E-5, ##*p* = 3.0E-5 by two-

700 sided Student's t-test. All comparisons refer to TAZ + elimusertib vs. elimusertib conditions,

701 except for G401 cells, in which comparison is for TAZ + elimusertib vs. TAZ. *n* = 5 replicates per

702 condition. (B-C) Synergy plots for combination treatment with TAZ (left axis) and elimusertib (right

703 axis) for (B) G401 and (C) ES1 cells. Cells were treated at the indicated doses for 9 days and

704 analyzed for synergy using the Zero Interaction Potency (ZIP) model. (D) Representative images

of G401 cells treated with the indicated treatment for 7 days. Elimusertib was added on Day 5.

705 Doses used were 500 mM TAZ and 100 nM elimusertib. (E) Quantification of γ H2AX fluorescence
706 relative to DAPI fluorescence. * $p = 9.3E-3$, ** $p = 6.2E-14$, *** $p = 1.5E-29$ by two-sided Student's
707 t-test. n = 332 nuclei for DMSO, 404 for TAZ, 400 for elimusertib, 257 for TAZ + elimusertib.

708

709

710

711

712

713

714

715

716

717

718

719

720

721

722

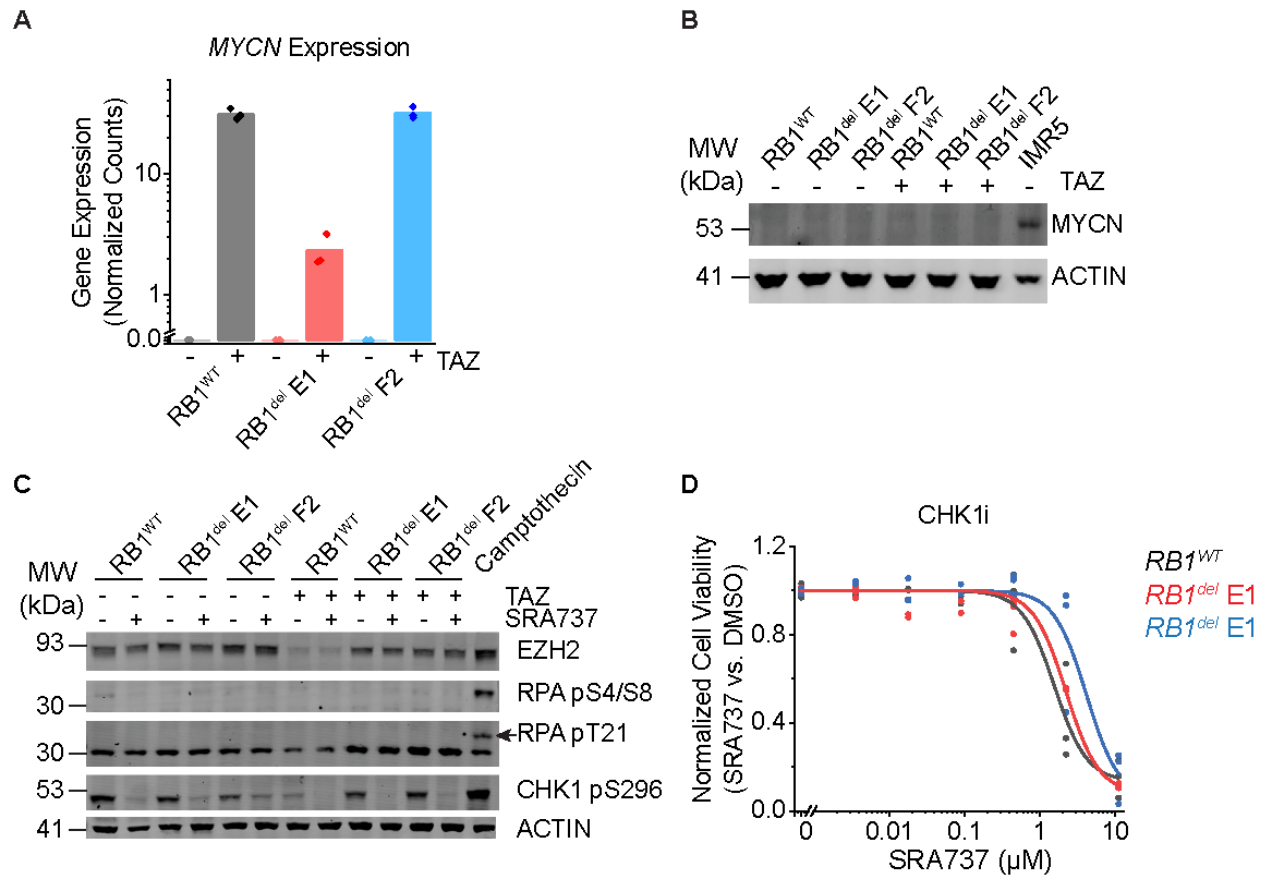
723

724

725

726

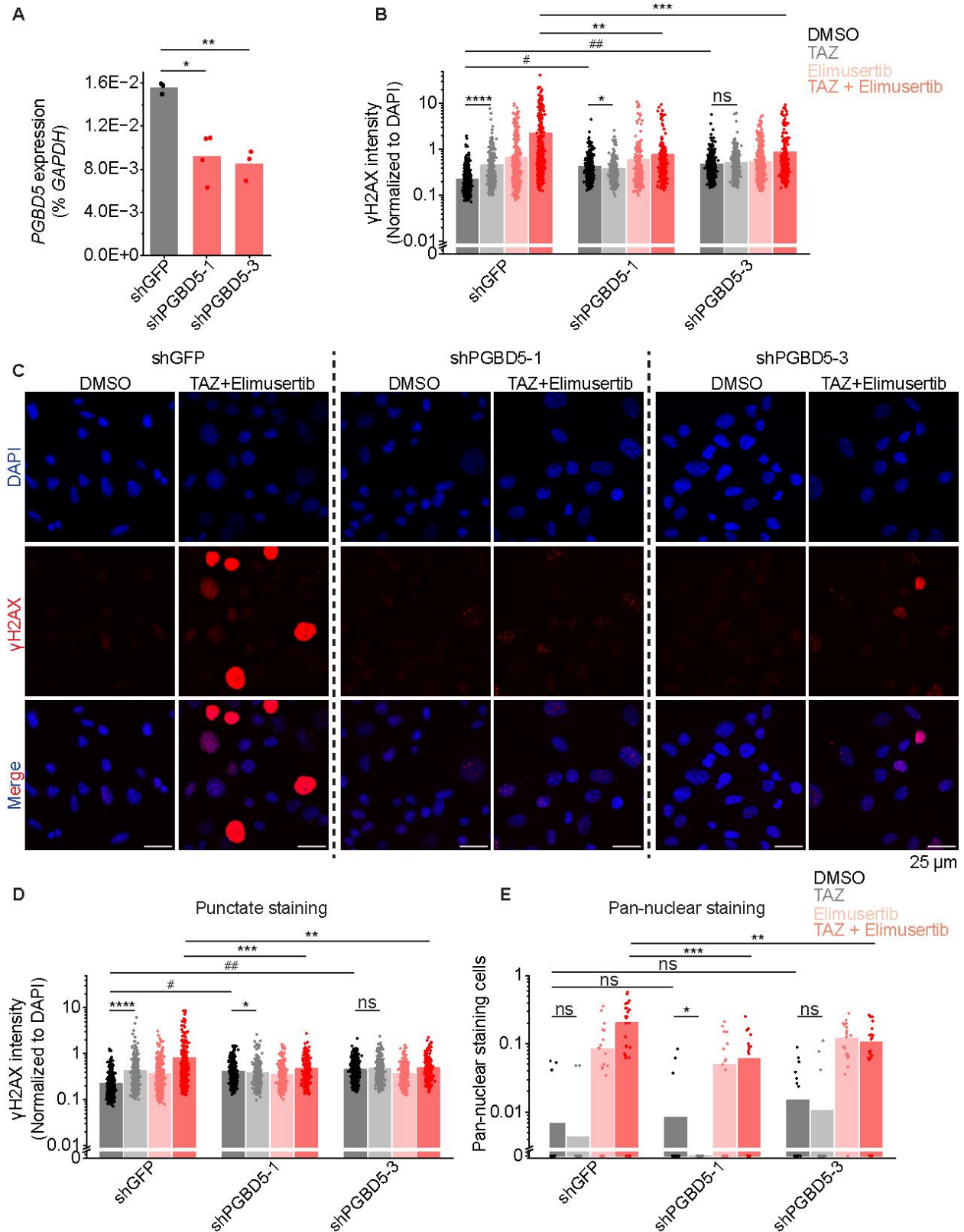
727



728
729

730 **Figure 3: CHK1 inhibition does not induce replication stress or synergize with TAZ:** (A)
 731 DESeq2-normalized read counts of cells treated with 10 μ M TAZ versus equivalent volume of
 732 DMSO for 11 days. n=3 biological replicates per condition. (B) Dose-response curves of G401
 733 cells treated with the CHK1 inhibitor SRA737 for 9 days. (C) Western blot assaying replication
 734 stress as measured by RPA phosphorylation at S4/8 and T21. Camptothecin treatment (1.5 μ M)
 735 for 2 h was used as a positive control for replication stress. Autophosphorylation of CHK1 at S296
 736 was used to confirm CHK1 inhibition. Cells were pre-treated with 10 μ M TAZ or DMSO for 9 days.
 737 Cells were then split and additionally treated with SRA737 (3 μ M) or equivalent volume of DMSO
 738 for 2 days. (D) Cells treated with 10 μ M TAZ or DMSO for 11 days do not express MYCN protein.
 739 MYCN-amplified neuroblastoma cell line IMR5 was used as a positive control for MYCN
 740 expression.

741
742
743

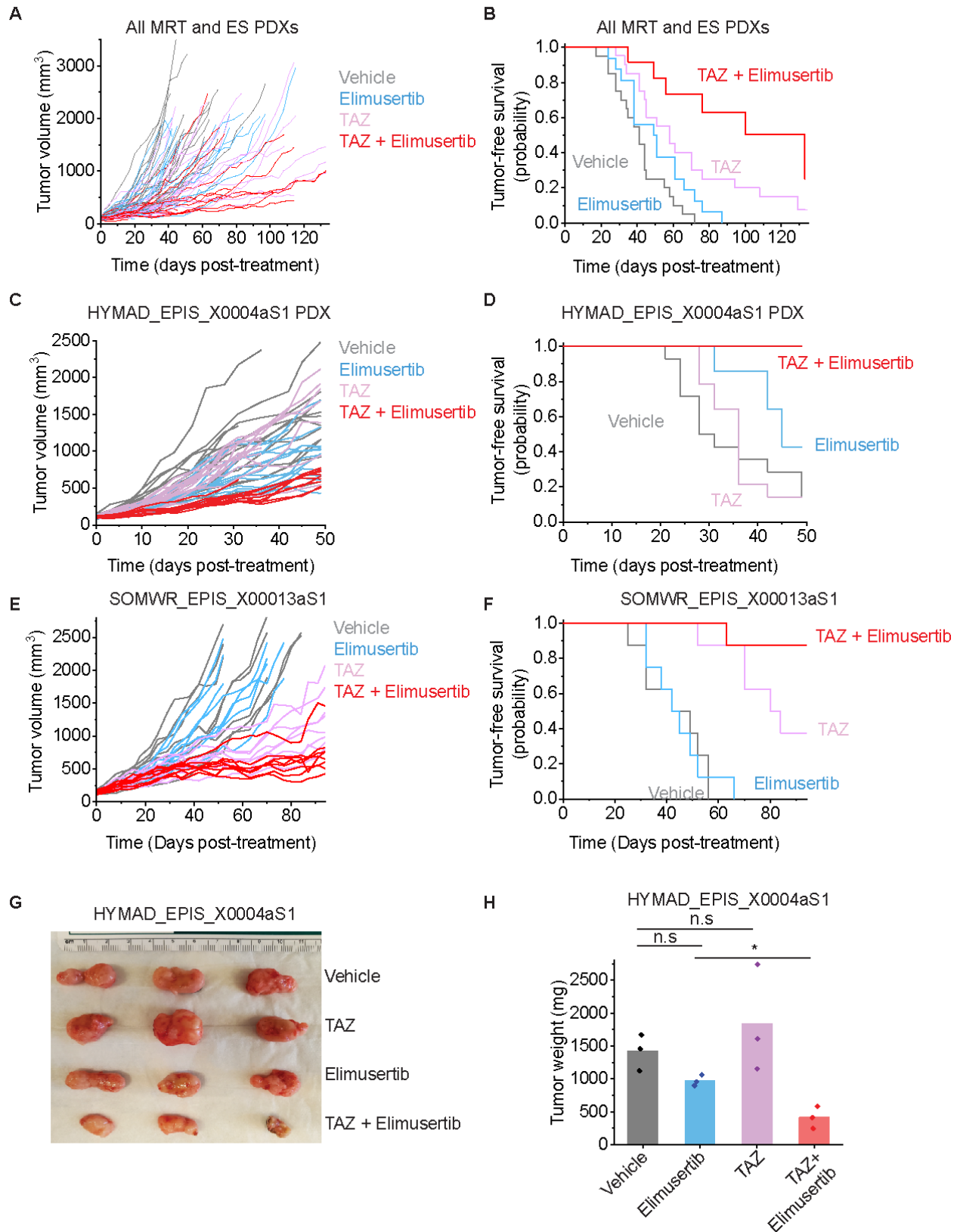


744

745 **Figure 4: TAZ-induced DNA damage is PGBD5-dependent:** (A) RT-qPCR showing *PGBD5*

746 expression vs. *GAPDH* in G401 cells with the indicated shRNA. * $p = 4.7E-3$, ** $p = 1.2E-3$. (B)

747 Quantification of γ H2AX fluorescence relative to DAPI fluorescence in all nuclei. $*p = 8.6E-3$, $**p$
748 $= 3.9E-8$, $***p = 4.4E-8$, $****p = 1.1E-12$, $\# p = 4.9E-34$, $## p = 4.0E-47$ by two-sided Student's t-
749 test. (C) Representative images of cells quantified in (B). (D) Quantification of γ H2AX
750 fluorescence relative to DAPI fluorescence in nuclei with punctate γ H2AX staining. $*p = 3.6E-2$,
751 $**p = 2.7E-5$, $***p = 2.4E-5$, $****p = 1.1E-15$, $\#p = 5.6E-51$, $##p = 1.7E-81$. For B-C, n for shGFP
752 cells is 539 for DMSO, 321 for TAZ, 491 for elimusertib, 418 for TAZ + elimusertib. n for shPGBD5-
753 1 is 497 for DMSO, 390 for TAZ, 354 for elimusertib, 277 for TAZ + elimusertib. n for shPGBD5-
754 3 is 703 for DMSO, 418 for TAZ, 554 for elimusertib, 317 for TAZ + elimusertib. (E) Proportion of
755 nuclei with pan-nuclear γ H2AX staining per field. Each dot represents one field. $*p = 9.2E-2$, $**p$
756 $= 1.6E-2$, $***p = 9.0E-4$ n for shGFP cells is 22 fields for DMSO, 22 for TAZ, 22 for elimusertib,
757 28 for TAZ + elimusertib. n for shPGBD5-1 is 22 for DMSO, 22 for TAZ, 22 for elimusertib, 20 for
758 TAZ + elimusertib. n for shPGBD5-3 is 22 for DMSO, 22 for TAZ, 20 for elimusertib, 22 for TAZ +
759 elimusertib.
760



762 **Figure 5: TAZ plus elimusertib improves therapeutic response in vivo:** (A) Tumor growth
763 curves for 5 mouse PDXs treated with the indicated drug regimen. $n = 20$ mice for vehicle and
764 elimusertib-treated groups, $n = 21$ for TAZ and TAZ + elimusertib-treated groups. Vardi U -test p
765 = $2.3E-2$ and 0.20 for combination vs. elimusertib or TAZ, respectively. (B) Kaplan-Meier curves
766 showing tumor-free survival (defined as tumor volume $\leq 1,000 \text{ mm}^3$) for the PDXs in panel C.
767 Mean survival is 51 days (95% CI: 42-60 days) for elimusertib, 68 days (95% CI: 53-82 days) for
768 TAZ to 100 days (95% CI: 74-124 days) for the combination. Log-rank test $p = 5.8E-4$ and $3.8E-$
769 2 for combination versus elimusertib or TAZ, respectively. (C) Tumor growth curves for the
770 HYMAD_EPIS_X0004aS1 PDX model treated with the indicated drug regimen. Vardi U -test $p =$
771 $2.0E-4$ for combination versus elimusertib or TAZ. $n = 14$ mice per treatment group. (D) Kaplan-
772 Meier curves showing tumor-free survival (defined as tumor volume $\leq 1,000 \text{ mm}^3$) for the PDXs
773 in panel C. Log-rank test $p = 6.2E-3$ and $6.3E-5$ for combination versus elimusertib or TAZ,
774 respectively. (E) Tumor growth curves for the SOMWR_EPIS_X00013aS1 PDX model. Vardi U -
775 test $p = 1.0E-3$ and $6.0E-2$ for combination versus elimusertib and TAZ, respectively. $n = 8$
776 mice for all groups. (F) Kaplan-Meier curves showing tumor-free survival (defined as tumor
777 volume $\leq 1,000 \text{ mm}^3$) for the SOMWR_EPIS_X00013aS1 PDX model; Mean survival is 90 days
778 (95% CI: 83-97 days) for combination versus 80 days (95% CI: 70-90 days) for TAZ and 45
779 days (95% CI: 37-52 days) for elimusertib. Log-rank test $p = 9.5E-5$ and $6.0E-2$ for combination
780 versus elimusertib and TAZ, respectively. (G) Image of representative tumors extracted from
781 mice in C-D and on Day 52 of treatment (H) their corresponding weights. $*p = 6.7E-3$ by two-
782 sided Student's t -test.
783